The 2010 IEEE/RSJ International Conference on
Intelligent Robots and Systems
October 18-22, 2010, Taipei, Taiwan

Reader Antennas' Configuration Effects for Two Wheeled Robots on Floor-Installed RFID Infrastructure - Analysis of Forward-Backward Configuration Effect -

Kenri KODAKA and Shigeki SUGANO

Abstract— **Reader antennas' configuration for two wheeled robots were evaluated to estimate their posture from floor-installed RFID tags. RFID systems where IC tags are installed under/on floors have widely been utilized in recent years as the next positioning infrastructure. The reader antennas should be properly placed on a robot so that such an environment can give full play to its potential capabilities of positioning the robot. This problem calls for guidelines in designing the configuration of reader antennas. Experiments using actual robots cannot offer sufficient data because of time and physical limitations, which prevent helpful and reproducible evaluations. We overcame this problem by constructing a simulation environment using a localization model and by evaluating the effects of configurations on positioning accuracy using computations. Of particular note, we found a "forward-backward configuration effect" from the results and had a detailed a discussion on how it occurred. Finally, a simple experiment using an actual robot validated the effect.**

I. BACKGROUND

There has been an urgent need in recent years to standardize the technology for positioning robots to enable them to be introduced into public spaces. A more compatible positioning infrastructure needs to be designed to construct systems with a high degree of interoperability. There is a model room called "the Human and Robot Symbiotic Space for Near-term Future Living" in our laboratory, where many RFID tags have been installed to estimate robot states (Fig. 1), simulating future home environments where robots interact symbiotically with humans[1]. IC tags can play the role of landmarks for moving robots by allowing them to refer to a table that lists these IC tag codes and their global positions. RFID technology has become very popular in studies of robots because it is robust against disturbances by such as lighting and obstacles, which adversely affect conventional methods that use cameras and ultrasonic waves. The decrease in the cost of these tags has also promoted this tendency.

Environments where IC tags are installed on/under the floor have widely been adapted in the field of positioning studies using the RFID system[2][3][4][5][6]. There are some advantages to arranging tags on/under the floor. First, we can easily arrange the tags in regular patterns and can easily manage all their global positions. Second, we do not need to take the effects of obstacles into account, which can be crucial problems in radio-wave sensing, when a reader's antennas are installed in the base of the robot. In addition,

The authors are with the WABOT-HOUSE Laboratory, Waseda University, Japan kenri@aoni.waseda.jp, sugano@waseda.jp

Fig. 1. RFID tags in model room (During Construction).

Fig. 2. Reader antenna and a tile of a cork mat with a tag

Fig. 3. Reproduced environment

such a positioning infrastructure can be freely moved and reproduced by adopting a resourceful approach in which tags are stuck to the tiles of a mat that can be connected to the same kind of mat. Actually, we could easily move and reproduce our positioning infrastructure in a remote location (e.g., exhibitions) and allow robots to operate in the same way as in our model room by sticking RFID tags to the tiles of a cork mat and connect them in any location (Fig. 1-3). In the light of these advantages, we think an environment with a floor equipped with regularly arranged RFID tags is one of the most probable positioning infrastructures.

How tags are arranged and where reader antennas (notated hereafter as RAs) are placed play an important role as environmental parameters in robot positioning. These parameters have been determined depending on the physical limitations of robots or the intuition of designers in most of the studies we cited. Positioning is generally more accurate if tags are arranged more densely and more readers are installed. However, arranging small tags densely over a wide space incurs expensive labor costs in having to install them and register their positions, and a reader system generally cost much more than tags. Therefore, it is very important to

improve the potential positioning resolution where there are limited resources for a RFID system when designing the infrastructure.

Kulyukin et al.[7] discussed a method of arranging a limited number of tags to prevent situations where a robot could not detect any tags when it navigated from point-to-point. However, their results indicated it was not simple for users to arrange the tags and it was quite impractical. Our previous study proposed a method of estimating the poses of robots using a particle filter[8][9]. We demonstrated in the study that positioning accuracy differed between several kinds of RAs' configurations. For example, orientation errors are not well predicted by rotating movement when RAs are placed near the center of the robot's rotation. The reason for this type of dead-zone, which is comparatively easy to understand, is that RAs cannot detect tags more than one very often in such situations. Also in case of straight movements, we could find an example where the predicting performance got worse when a single RA was placed backward in the robot. However, we could not collect enough our experimental data because of time and physical limitations, which prevented us from identifying the cause in detail.

This paper offers guidelines on how RAs should be placed in robots, thereby enabling us to obtain helpful and reproducible evaluations of configurations. We constructed a simulation environment that implemented the previously proposed method of localization and evaluated the configuration though computation. We especially picked up a "forward-backward configuration effect" in the result and have a detailed discussion on how it occurred. Finally, a simple experiment using an actual robot validated the effect.

This paper is organized as follows. Section II defines the RFID infrastructure we targeted in this paper. We describe how the pose of the robot was estimated using a particle filter in Section III. We present the simulation results in Section IV, and discuss these in Section V. Section VI describe an validation experiment using an actual robot. Finally, we conclude the paper in Section VII.

II. Target Environment

The section describes the properties of the RFID environment we targeted. As previously mentioned, it is practical to arrange RFID tags regularly in constructing a positioning infrastructure that has a high degree of interoperability. Therefore, we targeted an environment with a lattice of RFID tags, which seemed to be the simplest arrangement.

Here, let us define I_T as the arrangement interval and L_T as the tag antenna's width of a square ($L_T \leq I_T$), where a tag is placed on the center of a unit in the arrangement (see Fig. 4). For example, an interval of $I_T = 300$ mm and a width of $L_T = 260$ mm were used in our model room where about 350 RFID lattice-shaped tags (Hitachi Industrial Equipment System), each of which was 260 mm square, were placed at 300 mm intervals as shown in Fig. 1 (Note that the unit "mm" will be omitted from here on). Next, the configuration of the RAs is expressed as

$$\rho = \{X_{R_i} | X_{R_i} = (x_{R_i}, y_{R_i})^T\}_{1 \leq i \leq N_R} \quad (1)$$

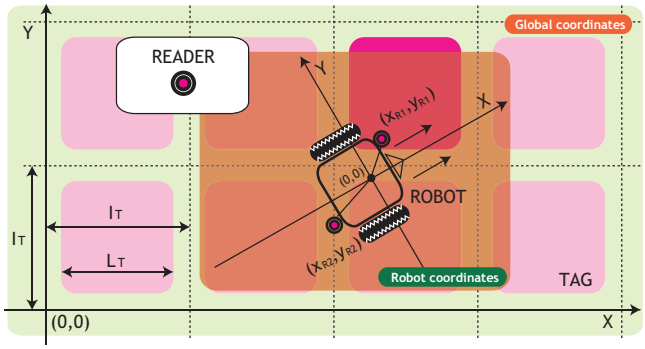

Fig. 4. Environmental parameters in two kinds of coordinate systems

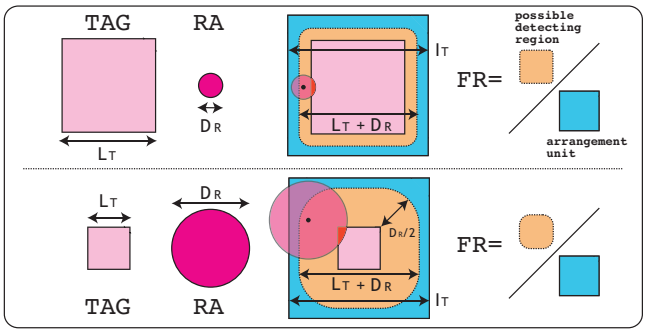

Fig. 5. Calculation of filling rate (FR)

In this equation, N_R denotes the number of RAs, and X_{R_i} represents the position of each RA in the robot's coordinates where the origin corresponds to the center of the robot's rotation and the X-axis positive direction corresponds to the forward direction of the wheels (Fig. 4). A RA is modelled as a circle whose diameter is notated as D_R (Fig. 5).

Here, we introduce an important assumption on detecting condition in the following.

Assumption on the detecting condition:

A necessary condition for a reader to detect a tag is that both the antennas have a common portion on a two-dimensional plane.

We have so far tried to use several kinds of RAs and tags and have found empirically that the above assumption is applicable approximately when the RA is enough close to a floor equipped with tags within less than about 50 mm. We construct a simulation environment based on the assumption in the following. It is generally difficult to formulate a detection probability with the detecting condition satisfied since the rate is quite changeable among situations. Therefore, we do not define a prior probability with an undetection event as a sensor model described in the next section.

In addition, we assume the following limitation for two kinds of antenna's sizes in the paper.

$$D_R \leq I_T - L_T \quad (2)$$

The limitation means that a RA cannot detect more than one tag. Although the RFID system is claimed to be able to detect multiple tags simultaneously, not many current technology has a collision-avoidance mechanism and no tags are read

as a result. We adopt the limitation so as to avoid such a situation.

We define a filling rate (FR) as a probability of satisfying with the detecting condition when a robot is randomly placed on a lattice of RFID tags (Fig. 5). The more FR is, the more chances of detection a RA has. FR is gotten by the simple geometrical calculation using both antenna's sizes as shown in the following,

$$\text{FR} = \frac{(L_T + D_R)^2 - \phi D_R^2}{I_T^2}, \tag{3}$$

where $\phi = (4 - \pi)/4 = 0.214\cdots$. Since neighboring FR value's environments generate almost the same shapes of the possible detecting region for the RA, we can approximately estimate the potential infrastructure capabilities (excluding RAs configuration) through following only the values of I_T and FR. Note that each antenna's size itself has no significant meaning in a predicting performance.

III. Localization model (particle filter)

This section describes an algorithm that is used to estimate a robot's pose on a lattice of RFID tags using Monte Carlo localization (MCL)[10], which has already been presented in our previous paper[8]. Typical process of updating particles is illustrated in Fig. 6 for an intuitive understanding.

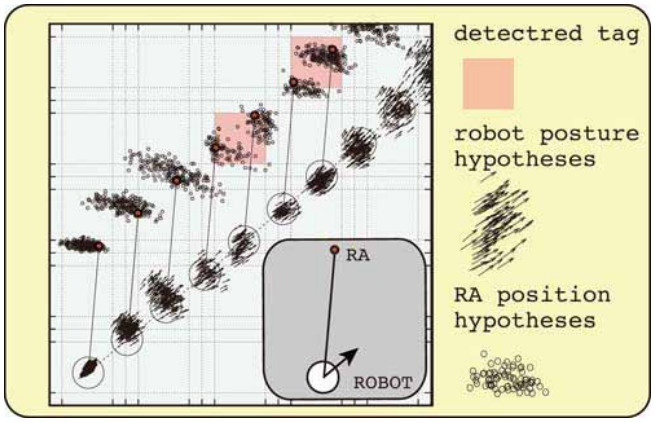

Fig. 6. Particles updating process.

A. MCL's procedure

Let $\mathbf{x}_t = [x_t, y_t, \theta_t]^T$ be the robot's state vector at the global coordinate at time t, and u_t and z_t be the vector of the encoder's value and detected tags at time t. The following steps are repeated to generate samples of N_p proportional to the distribution of $p(\mathbf{x}_t|z_{1:t}, u_{1:t})$.

1) Update particles by prediction using move model of $P(\mathbf{x}_t|u_t, \mathbf{x}_{t-1})$.
2) Update particles by correction using sensor model.
   a) Update weights of particles using $P(z_t|\mathbf{x}_t)$.
   b) Mix random particles using $P(\mathbf{x}_t|z_t)$.
   c) Update particles by resampling.

In this process, mixing random particles are especially useful for restoring from kidnapped conditions but we will not mix the random particles in the following simulation experiments because we only focused on factors related to the RAs configuration.

B. Move model

The odometry model adds noise to the actually derived signal of the encoder from $t-1$ to t notated as $u_t = [W_r, W_l]^T$ in the following,

$$\acute{u}_t = [rand(\gamma|W_r|), rand(\gamma|W_l|)]^{\mathrm{T}} + u_t, \tag{4}$$

where $rand(\bullet)$ generates a sample from a triangular distribution whose mean is zero, and whose standard deviation is $\bullet$[11]. In the equation, γ is closely related to the expected quality of the encoder. We will call γ **odometry noise rate** in the following. Each particle calculates its rotating distance according to Eq. 4, the corresponding robot posture is updated using an odometry with a tread value of the robot. The move model plays an important roll in making compensation to uncertainty of the robot movement. We can find that the model magnifies a possible region where a robot (and an RA) might be, as shown in Fig. 6.

C. Sensor model

The sensor model is designed based on the assumption of the detecting condition. When the prior probability is designed as a discrete function, which is exactly faithful to the detecting condition, all the weights of the particles out of a detected tag are set to zero. Such a design easily cause a kidnapped condition if environmental disturbance has occur or few number of particles are used. Therefore, we use the following sigmoid function as the sensor model.

The ith reader's position vector in the global coordinate system is given by

$$\mathbf{x}_{R_i,t}^{(2)} = \mathbf{x}_t^{(2)} + \begin{bmatrix} \cos\theta_t & -\sin\theta_t \\ \sin\theta_t & \cos\theta_t \end{bmatrix} X_{R_i}, \tag{5}$$

where $\mathbf{x}_t^{(2)}$ represents a two-dimensional positioning vector at time t and X_{R_i} is defined in the Eq. 1. We approximate the posterior probability of the measurement of $tag_{n_i,t}$ detected by the ith reader using

$$P(tag_{n_i,t}|\mathbf{x}_t) = Sg(D(tag_{n_i,t}, \mathbf{x}_{R_i,t}^{(2)}, D_R)) \tag{6}$$

$$Sg(l) = \frac{2}{1 + \exp(\lambda l)} \tag{7}$$

where $D(tag_{n_i}, \mathbf{x}_{R_i}^{(2)}, D_R)$ represents a minimum distance from the edge of the tag to the ith RA (which returns 0 if they are sharing common areas), and $Sg(l)$ is a discrete sigmoid function.

Assuming that the measurements of detection by the RA are independent, the resulting likelihood function can be calculated using

$$P(z_t = \{tag_{n_i,t}\}|\mathbf{x}_t) = \prod_i^{N_R} P(tag_{n_i,t}|\mathbf{x}_t) \tag{8}$$

If a RA cannot detect any tag ($tag_{n_i,t} = \phi$), the prior probability has a constant value, irrespective of what is the

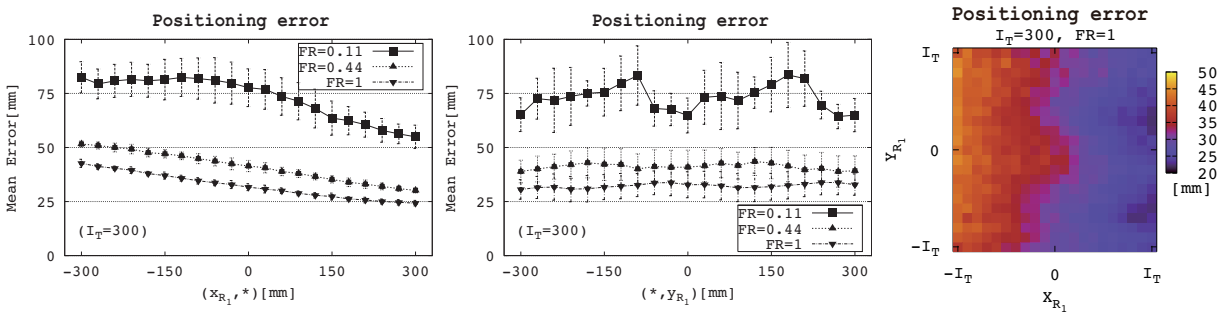

Fig. 7. Positioning errors in placing one RA. The left one plots mean errors when the RA's X-axis is fixed ($\frac{1}{21}\sum_{y_{R_1}} \mathbf{error}(x_{R_1}, y_{R_1})$), the middle one is with the RA's Y-axis fixed ($\frac{1}{21}\sum_{x_{R_1}} \mathbf{error}(x_{R_1}, y_{R_1})$), and the right one plots the mean errors distribution on two-dimensional plane in the robot coordinate system when FR is 1.0 ($\mathbf{error}(x_{R_1}, y_{R_1})$).

particle hypotheses. Resampling is done using low variance resampling[12] after normalizing the weights of the particles.

Intuitively speaking, these calculations correspond to an operation that clips out a RA's positioning region by a "window" of a detected tag, as shown in Fig. 6. Then λ in Eq. 7 functions as an important variable that determines how many particles out of the window survive. We have analyzed ranges of model parameters that can cope with the disturbances to some extent without failing regular accuracy, in the paper[9]. There we clarified that it is desirable that λ is set to around 10^{-1} and 10^{-2} with γ fixed to the actual encoder's quality. So we use λ as $\lambda = 10^{-1}$ in all the following experiments.

IV. Simulation

This section reports simulation experiments using the sensor model for the purpose of clarifying what effect the placement of RAs has on the resolution of positioning.

A. Experimental Design

We explain the environmental design. A two-wheeled robot with a tread of 400 mm is operated to move on a lattice of RFID tags, whose interval is fixed as $I_T = 300$, for 100 seconds from the initial posture given by $\mathbf{x}_0 = (0, 0, 0)$. The way of moving follows Table I. The actual rotation distance

TABLE I
Way of robot movement

time	way of moving	absolute wheel speed
$1 \leq t \leq 5$	Right rotating	$60 \sim 90$ (mm/s)
$6 \leq t \leq 25$	Forward moving	$60 \sim 90$ (mm/s)
$26 \leq t \leq 30$	Left rotating	$60 \sim 90$ (mm/s)
$31 \leq t \leq 50$	Forward moving	$60 \sim 90$ (mm/s)
$51 \leq t \leq 100$	$1 \leq t \leq 50$ is repeated	

at each wheel from $(t-1)$ to t is notated as $\mathbf{u}_t = [\mathbf{W}_r, \mathbf{W}_l]^T$ and the encoder's values are determined according to an encoder noise rate notated as γ_E.

$$u_t = [rand(\gamma_E|\mathbf{W}_r|), rand(\gamma_E|\mathbf{W}_l|)]^{\mathrm{T}} + \mathbf{u}_t \qquad (9)$$

One reader was placed somewhere among 21∗21 points in the robot coordinate such as $\{(x_{R_1}, y_{R_1}) = (30 * i, 30 * j)|i, j = -10, -9, -8, \cdots 10\}$. The RA was modelled as a point and three tag widths were used ($L_T = 100, 200, 300$). Then, the corresponding FR is 0.11, 0.44 and 1.0.

In this experiment, 10 % encoder noise was assumed and the odometry noise rate was set to the same value with the encoder noise rate ($\gamma = \gamma_E = 0.1$). 1000 particles, which are enough amount not to fall into a kidnapped condition, were used. Each particle had the correct hypothesis for the initial posture when the robot started to move. The detecting condition exactly follows the assumption described in Section II. The RA detected the tag satisfying with the condition without missing, if any, every second and the particles were simultaneously updated. The mean positioning error in the latter half of the motion was recorded for various 50 time series of the encoder's signal.

B. Results

Figure 7 plots the mean positioning errors in placing one RA. You can see an explanation on each figure in the caption.

Firstly, we can confirm that the more FR's value is, the better predicting accuracy is obtained. The errors do not change much when the placement of RAs moves along the Y-axis (middle). On the other hand, the change along the X-axis greatly affects the prediction performance with a negative inclination (left). We can see about double difference between the configurations of $x_{R_1} = I_T$ and $x_{R_1} = -I_T$, which should not be ignored in an actual implementation. We name the effect **"forward-backward (FB) configuration effect"** and discuss a cause of the effect in the following section.

V. Discussion

A. Analysis of experimental data

Figure 8 plots the robot and particles trajectories for the forward and backward configuration (FC and BC) during movement, as one of the experimental examples. We can see that the distribution of BC particles is more dispersed than that of FC. We analyzed the experimental data in detail and confirmed that the distribution of BC particles was largely spread out vertically against the moving axis even when the particles keep high weights. This implied that, for BC, high weights were allocated to many particles placed in the wrong

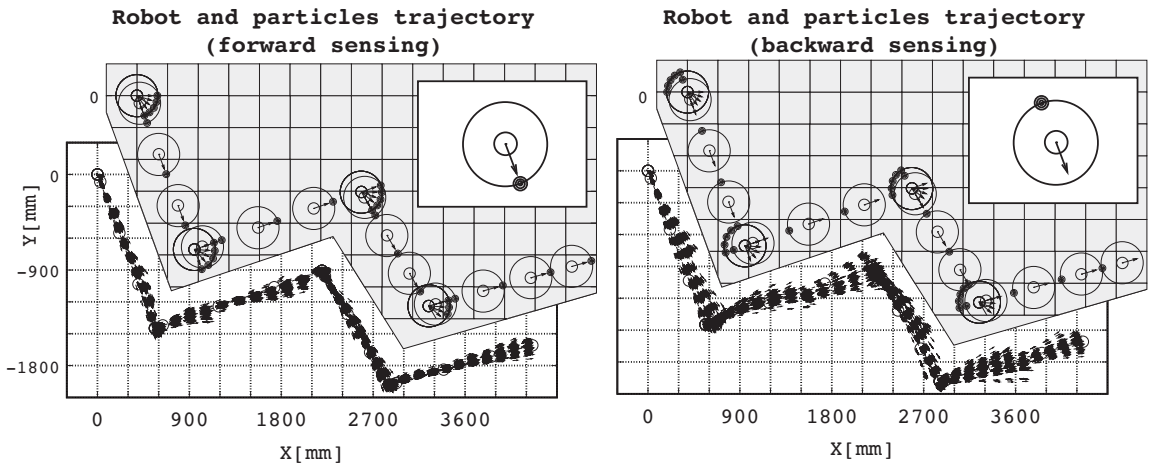

Fig. 8. Examples of robot and particles trajectories during 100 seconds movement by forward configuration ($\rho = \{(200, 0)^T\}$, left) and backward configuration ($\rho = \{(-200, 0)^T\}$, right). Randomly picked up 100 particles are plotted every 2 seconds.

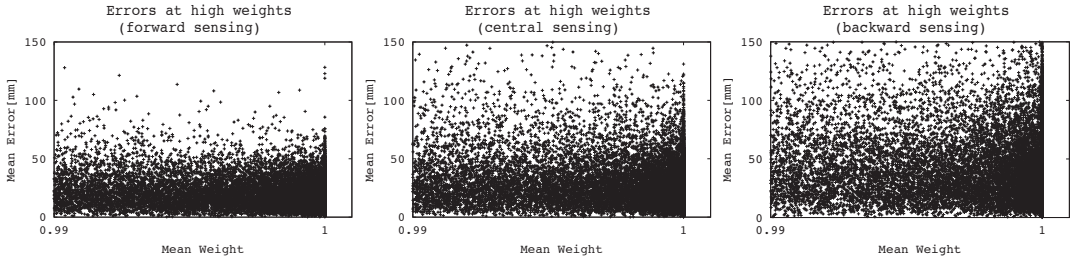

Fig. 9. Errors around the maximum weight. Each sample indicates a relation between mean error and weight at each time in the latter half of the movement and each figure collects the samples when x_{R_1} equals 300 (left), 0 (middle) , and -300 (right).

position, which prevented efficient resampling. To investigate this further, we collected positioning errors at weights around the maximum ($0.99 \sim 1.0$) in Fig. 9. We can see that maximum weight are frequently given to particles with errors of even about 100 mm in BC cases, while they are given to errors of less than about 50 mm in FC cases. This means that the region for the possible existence of the robot increases when BC is used.

In the following, we clarify the cause of this phenomenon based on our examination of the move model and provide a schematic proof of the FB configuration effect.

B. Schematic-proof of FB configuration effect

1) Wheel kinematics leads to "Expansion or Contraction effect" : A relation between the position and orientation of the robot updated during movement is not random but somewhat correlated depending on its own kinematics. We assumed each encoder's value to contain probabilistic error due to a triangular distribution (Eq. 4), which gives a regular uncertainty to changes in the robot's posture. This operation spreads out the robot's distribution (notated after this as $\mathcal{X}$) in the shape of a fan from the past position if there is no feedback from the sensor model (the middle of Fig. 10). Such spreads are the most common in move models of mobile robots because their characteristic is also caused by a universal designs where the error parameters of straight and rotating velocities are not significant different[12].

Here, we express the RA's positioning distribution mapped from the robot's distribution $\mathcal{X}$ as $\mathcal{R} = \Psi(\mathcal{X})$. Then, the degree of dispersion $\Psi(\mathcal{X})$ changes depending on the RA's configuration, as shown in Fig. 10. That is, **the FC makes the distribution expand while the BC makes it contract.** We will call this the **Expansion or Contraction (EC) effect** later and schematically represent it with the expression

$$\sigma(\mathcal{X}) > \sigma(\Psi_B(\mathcal{X})), \sigma(\Psi_F(\mathcal{X})) > \sigma(\mathcal{X}) \tag{10}$$

2) Reduction in EC effect by resampling: Figure 11 plots the degree of dispersion of $\mathcal{X}$ and the corresponding RA's distribution $\mathcal{R}$, where we have used the length of the major axis of a probability ellipse as the dispersion index, with the Mahalanobis distance fixed to 1. First, let us focus on the RA's distribution. We can see that the degree of dispersion expands slightly when its configuration changes from backward to forward. It is quite noticeable, however, that the changes are much less than those expected from the EC effect shown in Fig. 10. This is because the sensor model is a direct description of the topological relationship between the RA's positioning hypotheses and the detected tag. The sensor model clips out a possible positioning region for the RA by using a detected tag's window of an uniform size as shown in the Fig. 6, this does not depend on the configuration, i.e., **the resampling functions to unify the dispersion of** $\mathcal{R}$. This means the difference in the dispersion size due to the EC effect is reduced by the resampling effect.

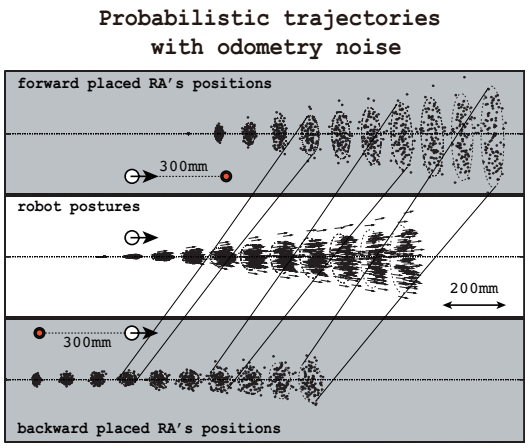

Fig. 10. Expansion or Contraction effect. Robot distribution $\mathcal{X}$ and corresponding RA distribution $\Psi_F(\mathcal{X})$ for configuration of $\rho = \{(300, 0)^T\}$ and $\Psi_B(\mathcal{X})$ for that of $\rho = \{(-300, 0)^T\}$ when robot moves straight ahead for 10 s at speed of 100mm/s, using same odometry noise rate as that in the experiment. The corresponding probability ellipses ($D = 2$) have also been illustrated. The $\sigma_D(\Psi_F(\mathcal{X}))/\sigma_D(\Psi_B(\mathcal{X}))$ is around 2.5 where σ_D means the length of the major axis of the ellipse.

We describe such coupling effects using expression

$$\frac{\sigma(\Psi_F(\Psi_B^{-1}(\mathcal{R}^{(B)})))}{\sigma(\mathcal{R}^{(B)})} \gg \frac{\sigma(\mathcal{R}^{(F)})}{\sigma(\mathcal{R}^{(B)})} \tag{11}$$

where $\mathcal{R}^{(F)}$ and $\mathcal{R}^{(B)}$ indicate the RA's distribution corresponding to FC and BC.

3) Proof: By applying the EC effect to $\mathcal{R}^{(F,B)}$, whose dispersion differences have mostly been absorbed, we can deduce the dispersion difference in the robot distributions notated as $\mathcal{X}^{(F,B)}$ that correspond to their configurations, which is another result given in Fig. 11, in the following.

$$\begin{aligned} \textbf{Eq.(11)} \quad &\Leftrightarrow \quad \sigma(\Psi_F(\mathcal{X}^{(B)})) > \sigma(\mathcal{R}^{(F)}) \\ &\Leftrightarrow \quad \sigma(\Psi_F^{-1}(\Psi_F(\mathcal{X}^{(B)}))) > \sigma(\Psi_F^{-1}(\mathcal{R}^{(F)})) \\ &\Leftrightarrow \quad \sigma(\mathcal{X}^{(B)}) > \sigma(\mathcal{X}^{(F)}) \end{aligned} \tag{12}$$

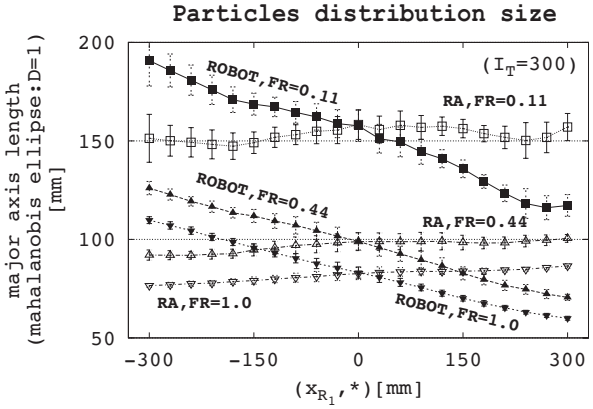

Fig. 11. Degree of dispersion of particles. (RA's X-axis is fixed.)

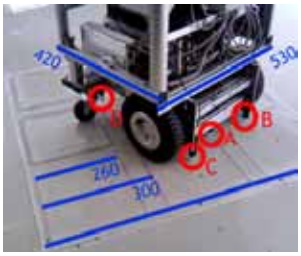

Fig. 12. WGH2

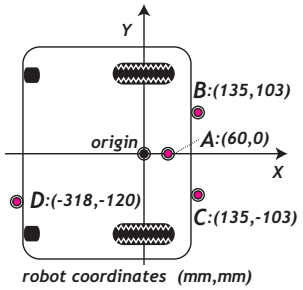

Fig. 13. Position of 4 Readers

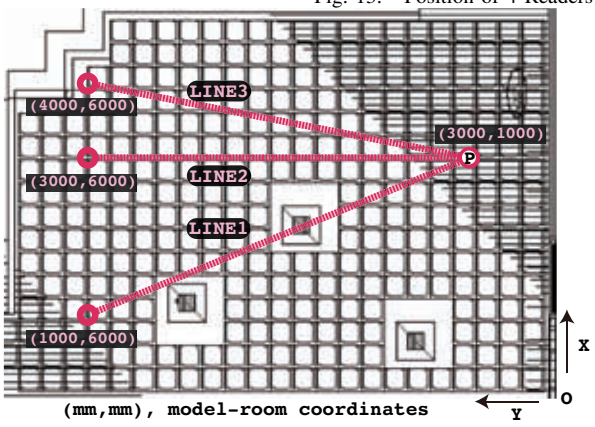

Fig. 14. Model room's layout and three kinds of moving lines of robots. The floor was equipped with about 350 RFID lattice-shaped tags (260×260 mm) placed at 300-mm intervals. Some blank spaces were put in the tags to enable installation of a few kinds of plumbing.

Here, we can regard $\sigma(\mathcal{X})$ as a possible existence region for where the robot is, and its increase results in making the position indefinite. This indefiniteness also results in increased error

$$\mathbf{error}(\mathcal{X}^{(B)}) > \mathbf{error}(\mathcal{X}^{(F)}) \tag{13}$$

This is a schematic proof of the FB configuration effect.

VI. Experiment in a Real Environment

We created a simple experiment using a real robot to determine the fitness of our discussion on the simulation for a real environment. We used a two-wheeled robot called WGH2 (Fig. 12), which has an encoder that monitors its rotation and can be equipped with reader antennas ($D_R = 15$, Hitachi Industrial Equipment System, Co., Ltd.) in four places (A-D, they simply depend on physical matter), and we let the robot move in our model room ($I_T = 300, L_T = 260, \mathrm{FR} = 0.84$, see Fig. 1). Each configuration in the robot coordinate system is as shown in Fig. 13

The robot was manually controlled in the experiment so as to shuttle on the same line for a comparison of the prediction accuracy between the forward and backward configuration (FC and BC) on nearly the same condition. **The backward-moving (BM) condition can be identified with the forward-moving (FM) with the X-axis of installed RAs converted to inverted values.** Therefore, we can determine the difference in performance between

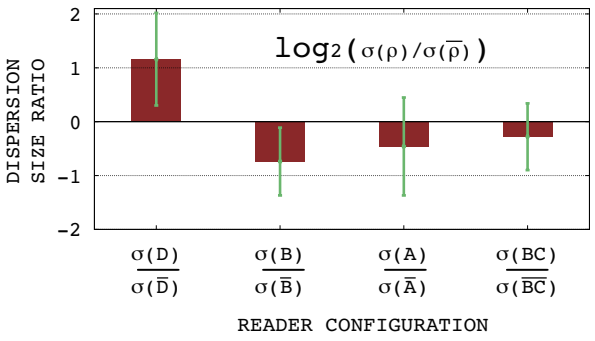

Fig. 15. Dispersion size ratio

the FC and BC by comparing data on the FM and BM. Moreover, we can achieve a quality control experiment by such a shuttle movement because each (forward or backward) movement enables the RA to detect potentially the same series of tags on the same moving line. The experiment used four RA configurations - ρ =A, B, D, BC - and the robot started from a point P (Fig. 14) and moved forward and backward (3 times) or back and forth (3 times) on each of three kinds of moving lines (LINE1, LINE2, and LINE3, see Fig. 14), at speed of $\pm$150mm/sec. (LINE2 was shifted laterally by 150 mm when A's configuration was used because the RA cannot detect any tags on such a condition.) Measuring accurate positioning errors during the movement is difficult, so the mean dispersion size of the particle's distribution was recorded instead. The ratio of the dispersion size (**DS_RATIO**) between the FM and BM in a single shuttle movement was calculated as an accuracy indicator, as shown in the following,

$$\textbf{DS\_RATIO} = \log_2(\sigma(\rho)/\sigma(\bar{\rho})), \tag{14}$$

where $\sigma(\rho)$ and $\sigma(\bar{\rho})$ are the length of the major axis of a probability ellipse of the distribution during FM and BM with ρ's configuration, respectively. As mentioned previously, the distribution size reflects a possible region where the robot might be. Therefore, a positive **DS_RATIO** implies the BM's positioning accuracy is better than the FM's positioning accuracy, and a negative value implies the opposite.

In this experiment, we added an algorithm of mixing random particles so as to enable the initial particles to obtain hypotheses properly and to avoid kidnapped conditions. The mixing rate was followed by the sensor resetting method[13], where the threshold of the mean weight of particles for mixing was set to 10^{-1}. The particles were updated every half second with $N_P = 200, \lambda = 10^{-1}, \gamma = 0.15$.

Figure 15 indicates each configuration's average **DS_RATIO** for 18 shuttle movements (9 forward and backward / 9 back and forth). On the whole, we found that the dispersion size increases where the RA can be regarded as being placed backward ($\mathrm{D}, \bar{\mathrm{B}}, \bar{\mathrm{A}}, \overline{\mathrm{BC}}$), and the tendency increases when the RA's absolute value of the X-axis is magnified. Specifically, the ratio is about double when D's configuration is used. The results support the validity of our simulation discussion.

VII. Conclusion

This paper discussed how RAs should be placed for accurate positioning on floor-installed RFID tags. A simulation experiment extracted the forward-backward configuration effect, which can be important clues to designing a single RA's configuration. Moreover, we discussed the cause of the problem in detail and clarified that it results from coupling effects between the "EC effect" based on the wheel kinematics and the resampling process that unifies the dispersion of the RA's distribution. Our experiment using the actual robot supported the validity of the discussion.

This paper assumes a simple detecting condition. Therefore, we think our discussions are widely applicable to localization methods using landmarks on/under the floor.

VIII. Acknowledgments

This project could not have been completed without the cooperation of the Gifu Prefecture. We would sincerely like to express our profound appreciation for their cooperation.

References

[1] S. Sugano, Y. Shirai, and S. Chae: "Environment Design for Human-Robot Symbiosis - Introduction of WABOT-HOUSE Project" *Proc. of the 23rd Int. Symposium on Automation and Robotics in Construction*, pp.152-157, 2006.

[2] K. Kodaka, H. Niwa, Y. Sakamoto, M. Otake, Y. Kanemori, and S. Sugano: "Transport Services on Indoor Map Generating System using Spatially Distributed RFID Tags for Home Environment", *Proc. of the IEEE/ASME International Conference on Advanced Intelligent Mechatronics (AIM)*, pp.758-763, 2009.7

[3] B. K. Kim, N. Tmokuni, K. Ohara, T. Tanikawa, K. Ohba, and S. Hirai "Ubiquitous Localization and Mapping for Robots with Ambient Intelligence", *Proc. of the IEEE/RSJ International Conference on Intelligent Robots and Systems (IROS)*, pp.4809-4814, 2006.

[4] T. Asakawa, K. Nishihara, and T. Yoshidome: "A Detection System of Location and Direction Angle by a RF Tag Reader Using a Rotary Antenna", *Transactions of the Japan Society of Mechanical Engineers. C (Japanese)*, Vol.73, No.729, pp.1494-1500, 2007.

[5] S. Park, R. Saegusa, and S. Hashimoto: "Autonomous Navigation of a Mobile Robot Based on Passive RFID", *Proc. of the IEEE International Symposium on Robot & Human Interactive Communication (ROMAN)*, pp.218-223, 2007.

[6] K. Murakami, T. Hasegawa, R. Kurazume, and Y. Kimuro: "Supporting Robotic Activities in Informationally Structured Environment with Distributed Sensors and RFID Tags", *Journal of Robotics and Mechatronics*, Vol.21, No.4 pp.453-459

[7] V. Kulyukin, A. Kutiyanawala, and M. Jiang: "Surface-embedded Passive RF Exteroception: Kepler, Greed, and Buffon's Needle", *Proc. of the Ubiquitous Intelligence and Computing (UIC)*, pp.33-42, 2007.

[8] K. Kodaka, H. Niwa, Y. Sakamoto, M. Otake, Y. Kanemori, and S. Sugano: "Pose Estimation of a Mobile Robot on a Lattice of RFID Tags", *Proc. of the IEEE/RSJ International Conference on Intelligent Robots and Systems (IROS)*, pp.1385-1390, 2008.

[9] K. Kodaka, H. Niwa, Y. Sakamoto, and S. Sugano: "Robot Pose Estimation on Floor Equipped with a Lattice of RFID Tags", *Jouranl of Society of Instrument and Control Engineers (japanese)*, Vol.45, No.7, pp.379-387, 2009

[10] D. Fox, W. Burgard, F.Dellaert and S. Thrun: "Monte Carlo localization for mobile robots", *Proc. of the IEEE International Conference of Robotics and Automation (ICRA)*, pp.1322-1328, 1999

[11] G. Winkler: "Image Analysis, Random Fields, and Dynamic Monte Carlo Methods", *Berlin: Springer Verlag*, 1995

[12] S. Thrun, W. Burgard, D. Fox: "Probabilisic robotics", *Massachusetts Institute of Technology*, I-4.3, I-5.3, 2006

[13] S. Lenser, and M. Veloso: "Sensor Resetting Localization for Poorly Modelled Mobile Robots", *Proc. of the IEEE International Conference of Robotics and Automation (ICRA)*, pp.1225-1232, 2000